Heliyon 8 (2022) e12145

Contents lists available at ScienceDirect

Heliyon

journal homepage: www.cell.com/heliyon

Research article

Efficient enhancement on crystallization and electrochemical performance of $LiMn_2O_4$ by recalcination treatment

Jiabin Hao, Siqi Hao *, Mu Xie

Department of Chemical Engineering, Hebei Petroleum University of Technology, Chengde 067000, PR China

HIGHLIGHTS

- The spinel R-LMO cathode material was successfully prepared by recalcination treatment process.
- The R-LMO present the selective growth of the (110) and (100) crystal planes.
- The R-LMO displays the better electrochemical performance than that of P-LMO.

ARTICLE INFO

Keywords:
Energy storage and conversion
Crystal growth
Lithium-ion batteries
Spinel $LiMn_2O_4$
Recalcination treatment

ABSTRACT

Spinel $LiMn_2O_4$ cathode material was obtained by a recalcination treatment, which exhibits excellent crystallization and electrochemical performance. A series of test and analysis results revealed that the performance enhancement of as-prepared sample is related to the crystal structure, morphology and electrochemical properties. Owing to the recalcination treatment, the spinel $LiMn_2O_4$ presents a truncated-octahedral morphology with selective growth of the (110) and (100) crystal planes, which would effectively inhibit manganese dissolution. Moreover, the optimized sample exhibits a better crystallinity and electrochemical reversibility than that of pristine sample, which can provide a faster Li ion de-intercalation/intercalation kinetics. Hence, the spinel $LiMn_2O_4$ cathode material delivers a high initial discharge capacity of 112.3 $mAh{\cdot}g^{-1}$ with a good capacity retention of 90.3% after 500 cycles and an excellent rate performance. This study constructed a facile and meaningful method to prepare spinel $LiMn_2O_4$ cathode material, which may facilitate the development of lithium-ion batteries.

1. Introduction

Spinel $LiMn_2O_4$, the cathode materials in lithium-ion batteries, have exhibited unusual properties such as three-dimensional lithium-ion diffusion channels, great rate capability and relatively high operating voltage [1, 2, 3]. Despite some advantages, $LiMn_2O_4$ cathode material suffers from fading capacity and poor electrochemical performance, which mainly because of Jahn-Teller distortion, the dissolution of Mn ions and oxygen defects [4, 5]. Several synthesis methods, including solid-state method, sol-gel process, microwave sintering method, hydrothermal synthesis, co-precipitation have been used to obtain the spinel $LiMn_2O_4$ with improved electrochemical performance [6, 7, 8, 9, 10]. Xiang and co-workers reported a low-temperature solid-state combustion method to produce spinel $LiMn_2O_4$ cathode material [6]. Zhao et al. prepared successfully prepared the spinel $LiMn_2O_4$ cathode material with octahedral particles via a low-cost and eco-friendly method. At high rate of 10 C, this material delivered 85.7 $mAh{\cdot}g^{-1}$ discharge capacities with excellent retentions of 94.7% after 200 cycles [7]. Yao and co-workers obtained the $LiMn_2O_4$ material by sol-gel method, where the sample calcined at 750 °C had high crystallinity, good dispersion and excellent electrochemical properties than that of other samples calcined at 550 °C and 650 °C [8]. However, these methods not only have complicated synthesis process, but also long reaction time, which will affect the large-scale production of materials.

This work reports recalcination treatment to fabricate $LiMn_2O_4$ cathode material with enhanced crystallinity and electrochemical performance [11, 12]. As a result, the $LiMn_2O_4$ prepared by recalcination treatment delivered much higher cyclic and rate performance in lithium-ion batteries. The crystallinity, kinetics and electrochemical properties of the $LiMn_2O_4$ cathode material were investigated by X-ray

* Corresponding author.
E-mail address: haosiqi_cdpc@163.com (S. Hao).

https://doi.org/10.1016/j.heliyon.2022.e12145
Received 19 September 2022; Received in revised form 28 September 2022; Accepted 29 November 2022

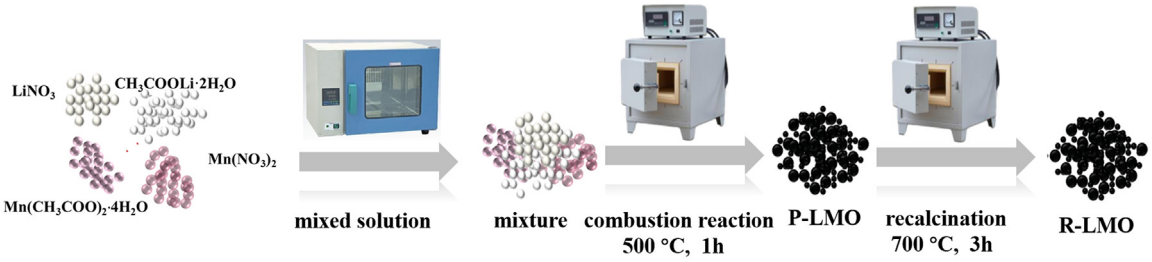

Figure 1. A set of photos of the processes for preparing the P-LMO and R-LMO cathode materials.

diffraction, scanning electron microscope and other tests. The related reasons for crystallization and electrochemical performance of $LiMn_2O_4$ by recalcination treatment are discussed. The methods above provided an important technical process for the spinel $LiMn_2O_4$ cathode material with the excellent crystallinity and electrode with high cycling performance.

This work indicates the recalcination treatment strategy has vital significance to promote the practical application of spinel $LiMn_2O_4$.

2. Experimental section

2.1. Materials preparation

Spine $LiMn_2O_4$ cathode material was prepared by recalcination treatment process. In this work, 4 g $LiMn_2O_4$ target product can be prepared, using 0.7625 g $LiNO_3$ (AR, Aladdin, 99.0%) and 1.1284 g $CH_3COOLi{\cdot}2H_2O$ (AR, Aladdin, 99.0%) as lithium precursor 3.9587 g $Mn(NO_3)_2$ (AR, Aladdin, 99.0%) and 5.4218 g $Mn(CH_3COO)_2{\cdot}4H_2O$ (AR, Aladdin, 99.0%) as manganese precursor, keeping the molar ratio of CH_3COO^-:NO_3^- = 1:1. The mixed raw material was removed into an oven at 100 °C for 10 min to form the homogeneously mixture solution. Subsequently, the solution generates an autoxidative combustion reaction at 500 °C for 1 h to form pristine $LiMn_2O_4$ (noted as P-LMO). In order to improve the crystallinity of the material, the P-LMO power was recalcined at 700 °C for 3 h to obtain recalcination $LiMn_2O_4$ cathode material (R-LMO). The above process diagram is shown in Figure 1. The mass loading of the electroactive materials on the working electrode was about 1.0 mg/cm^2.

2.2. Lithium-ion batteries synthesis

The spinel $LiMn_2O_4$ cathode material, conductive carbon black and polyvinylidene fluoride (PVDF) were mixed in a N-methyl-pyrrolidone (NMP) solvent in a weight percentage of 80:10:10 to prepare a slurry. Then the mixed slurry was uniformly coated on the aluminum foil collector by a doctor-blade technology to get the cathode film. The cathode films were cut into discs with a diameter of 16 mm, and then dried in a vacuum drying oven at 120 °C for 8 h. The CR2025 batteries were assembled in a high purity argon glove box, in which lithium metal, 1 M $LiPF_6$ in EC/DMC (1:1 in volume) and Celgard 2320-type membrane were used as anode, electrolyte and separator, respectively.

2.3. Characterization techniques

X-ray diffraction (XRD) test were carried out by an X-ray power diffractometer (D8 ADVANCE, BRUCKER) in 2 range of 10–70°. The morphological properties and lattice structure of the samples were characterized by the scanning electron microscope (SEM, NOVA NANOSEM 450, America FEI) and transmission electron microscope (TEM, JEM-2100). The lithium-ion batteries were cycled by a galvanostatical charge-discharge tests were measured by the Land electric test system CT2001A (Wuhan Jinnuo Electronic Co., Ltd) in the voltage from 3.0 to 4.5 V (versus Li/Li$^+$). The cyclic voltammetry (CV) and electrochemical impedance spectroscopy (EIS) were carried out by an electrochemical workstation (CHI660D, Shanghai Chenhua, China). The scan rate and potential region are 0.1 mV/s and 3.6–4.5 V, respectively. The frequency range is from 100 kHz to 1.0 Hz.

3. Result and discussion

In order to evaluate the electrochemical performance of the $LiMn_2O_4$ electrodes, the constant current charge and discharge test is carried out. Figure 2(a) shows the cycling curves of P-LMO and R-LMO samples in lithium-ion batteries at 0.5 C. Owing to the recalcination treatment, the R-LMO electrode delivers higher initial capacity of 112.3 mAh·g^{-1} than that of P-LMO (106.1 mAh·g^{-1}). The corresponding initial galvanostatic charge-discharge curves of the P-LMO and R-LMO electrodes are provided in Figure S1(b). As seen, both of the samples display two obvious charge-discharge platforms, corresponding to the Li$^+$ insertion/extraction process in spinel $LiMn_2O_4$, which correspond to the two-phase equilibrium of λ-MnO_2/$Li_{0.5}Mn_2O_4$ and single-phase equilibrium of $Li_{0.5}Mn_2O_4$/$LiMn_2O_4$, respectively [10, 12]. Importantly, the discharge voltage plateaus of the R-LMO sample are higher than that of the P-LMO sample, which may be related to the optimization of the Li$^+$ insertion/extraction behaviors. After 500 cycles, the discharge capacity of P-LMO and R-LMO electrode decrease to 89.6 mAh·g^{-1} and 101.4 mAh·g^{-1}, with 84.4% and 90.3% capacity retention, respectively. The cycle tests of the samples are further performed at 2 C, shown in Figure S1(a). The R-LMO sample delivers high initial capacity of 111.7 mAh·g^{-1}, retaining 103.0 mAh·g^{-1} after 100 cycles. While the discharge specific capacity of the P-LMO sample decreases from the initial discharge capacity 107.0 mAh·g^{-1} to 80.1 mAh·g^{-1}. As known, the cyclic stability is associated with Mn dissolution, especially at high current rate [13]. In this regard, the long cycle performance of the P-LMO and R-LMO is performed at 5.0 C, as shown in Figure 2(b). The R-LMO sample delivers the initial capacities of 104.3, obtaining the retention rate of 89.5%, which are higher than 95.7 mAh·g^{-1} and 76.9% of the P-LMO electrode, respectively. Figure 2(c) describes the rate cycling curves of the P-LMO and R-LMO samples at the current rate from 0.5 C to 10.0 C. The discharge capacity decreases gradually when the current rate creases from 0.5 C to 2.0 C. However, from 5.0 C and 10.0 C, especially at 10.0 C, R-LMO sample obviously exhibits a higher discharge capacity of 70.9 mAh·g^{-1} than that of the P-LMO sample (47.1 mAh·g^{-1}). While the current density returns back to 0.5 C again, the reversible capacity of 98.7% of the original capacity of 109.1 mAh·g^{-1} is still retained, proving a superior reversibility, as shown in Figure 2(d), which occurs probably related to Mn dissolution decrease in the crystal truncated octahedron R-LMO with (110) and (100) crystal surfaces. To further compare the electrochemical performance of the $LiMn_2O_4$ between our work and those previous work reported in literature, and the comparison results are listed in Table S1. It is clearly seen that the R-LMO displays more excellent or comparable electrochemical performance than that of the other LMO samples at the same discharge rate. This study constructed a facile and meaningful method to prepare spinel $LiMn_2O_4$ cathode material, which may facilitate the development of lithium-ion batteries.

The morphology of P-LMO and R materials are displayed in Figure 2. As seen, the P-LMO material shows an irregular particle morphology with

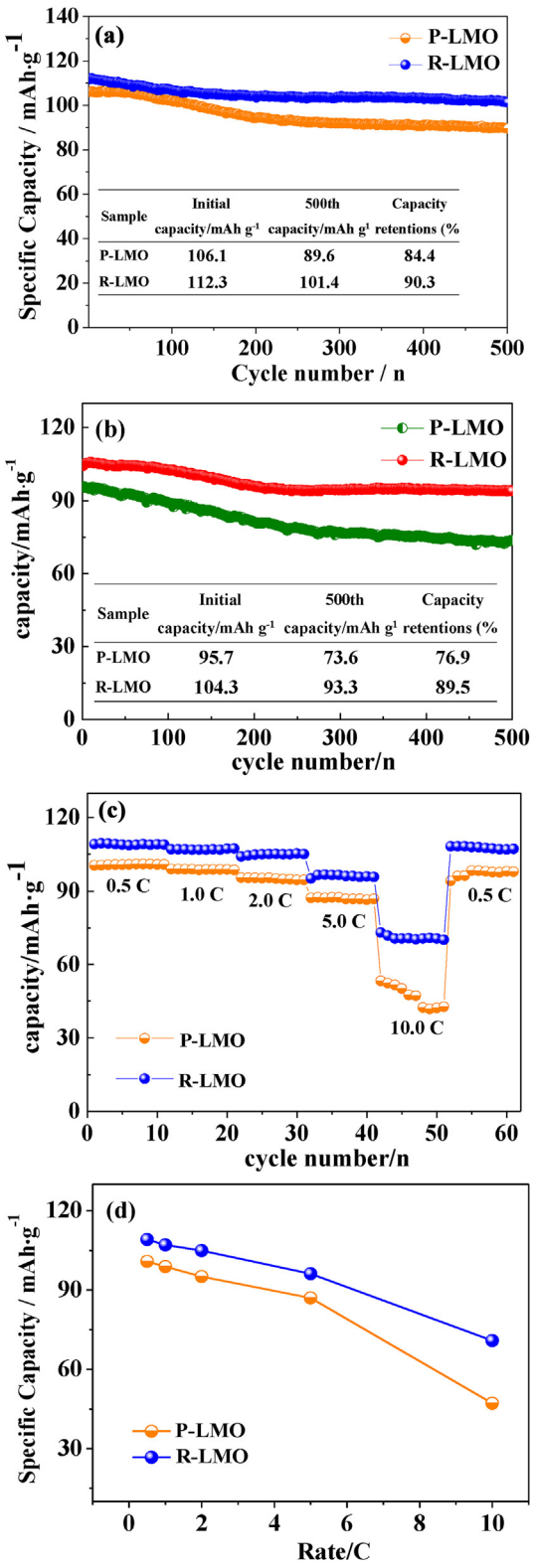

Figure 2. (a) The cycling performance curves at 0.5 C, (b) 5.0 C, (c) Rate capability at 0.5 C–10.0 C and (d) The trend curves of rate performance of P-LMO and R-LMO samples (1 C = 148 mAh·g^{-1}).

severe particle agglomeration in Figure 3(a). Compared to the P-LMO material, the R-LMO material exhibits a typically truncated octahedral structure, and the particles were uniformly dispersed with a diameter of about 200 nm in Figure 3(b). Such results indicate that recalcination process makes the combustion reaction complete, which is beneficial to crystal growth of spinel $LiMn_2O_4$. Furthermore, the high-temperature recalcination promotes the selective growth of the (110) and (100) crystal planes in $LiMn_2O_4$ material shown in Figure 3(c), which expands the diffusion channels of lithium ions to improve the electrochemical performance of the batteries [14]. Figure 3(d) displays the TEM image of the R-LMO material, and further confirming the truncated octahedral structure, in which the most surfaces are aligned with the

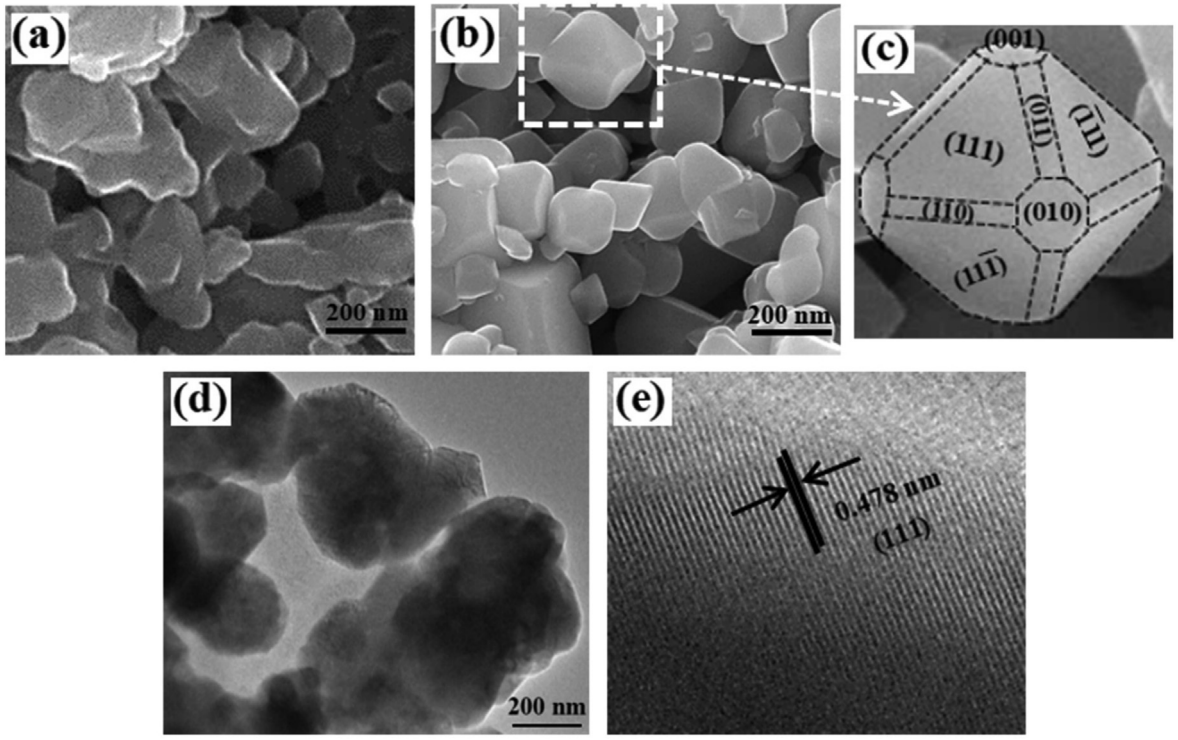

Figure 3. SEM images of the (a) P-LMO sample, (b)R-LMO sample, (c) the truncated octahedral morphology of the R-LMO sample, (d) TEM image and (e) HRTEM image of the R sample.

crystallographic orientation with minimal Mn dissolution [15]. As shown in Figure 3(e), the lattice space distance of 0.478 nm of R material is in accordance with the (111) plane of the spinel $LiMn_2O_4$. Hence, the excellent crystallinity and unform morphology of R-LMO material can lead to a better cycling and rate performance.

The X-Ray diffractograms (XRD) can well demonstrate that both P-LMO and R-LMO samples have the typical cubic spinel $LiMn_2O_4$ structure with the F*d3m* space group (JCPDS No. 35-0782) shown in Figure 4. Obviously, impurity phase of Mn_2O_3 and Mn_3O_4 still exists in P-LMO sample, while R-LMO sample exhibits pure spinel $LiMn_2O_4$ crystal phase. Therefore, the recalcination treatment can lead to a better crystallinity, indicating a better electrochemical performance of R-LMO than that of P-LMO electrodes.

To investigate the change of inner impedance for the P-LMO and R-LMO electrodes, the Electrochemical impedance spectroscopy (EIS) analysis with a frequency range is from 100 kHz to 1.0 Hz is adopted. Figure 5(a) gives the Nyquist diagrams of the P-LMO and R-LMO electrodes before cycle at 0.5 C. The corresponding equivalent circuit was

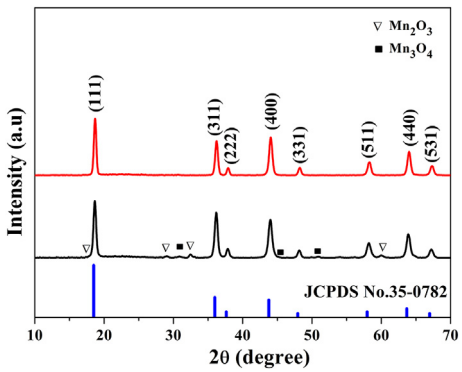

Figure 4. XRD patterns of P-LMO and R-LMO electrodes.

obtained by the Zview software simulation, as shown in Figure 5(b). Where the R_s and R_{ct} represent the ohmic resistance and the charge-transfer resistance, respectively. CPE and W_o are the double-layer capacitor and the Warburg impedance [16]. The R-LMO sample has a lower R_{ct} value of 159.0 Ω than that of P-LMO sample (219.5 Ω), indicating the faster charge transfer and leading to better rate capability. Figure 5(c) gives the fitting curves of real parts of the complex impedance (Z′) and $\omega^{-0.5}$, showing a good linear relationship and giving the slope value σ_w. Furthermore, the Li ion diffusion coefficient (D_{Li}^{+}) can be obtained according to the following formula [17, 18]:

$$Z' = R_s + R_{ct} + \sigma_w \omega^{-0.5} \quad (1)$$

$$D_{Li}^{+} = R^2T^2/2A^2n^2F^4C^2\sigma_w^2 \quad (2)$$

where R-LMO is the gas constant (8.314 J/mol K), T is the absolute temperature (298.15 K), A is the surface area of the electrode (cm^2), n is electron transfer number for electrode reaction, F is the Faraday constant (96,484.5 C/mol), C is the concentration of Li ion in the electrode (0.02378 mol/cm^3). Depending on formula (1formula (1) and (2)(2), the R-LMO sample has a larger D_{Li}^{+} value of 1.91×10^{-14} cm^2/s than that of P-LMO sample (1.57×10^{-14} cm^2/s), indicating a faster Li ion diffusion process in the R electrode. This is consistent with the above cycling and rate performance results.

To investigate the reversibility and kinetics of the P-LMO and R-LMO electrodes, Figure 6(a) and (b) give the CV curves of the P-LMO and R samples at various scan rates from 0.05 mV s^{-1} to 0.5 mV s^{-1} to study the effect of scan rates, where the shape of the peaks becomes flat and peak current increases in sequence with the increase of scan rates. However, the peaks of the P-LMO sample shows deformed and drifted. A good liner relationship between peak current density and square root of the scan rate in R-LMO sample is shown in Figure S3, suggesting a diffusion-controlled kinetics of Li ion deintercalation/intercalation process [19, 20]. Moreover, the cyclic voltammograms (CV) test of P-LMO and R samples was carried out in the voltage of 3.6–4.5 V with a scan rate of 0.05 mV s^{-1} shown in Figure S2. Obviously, two pairs of similar

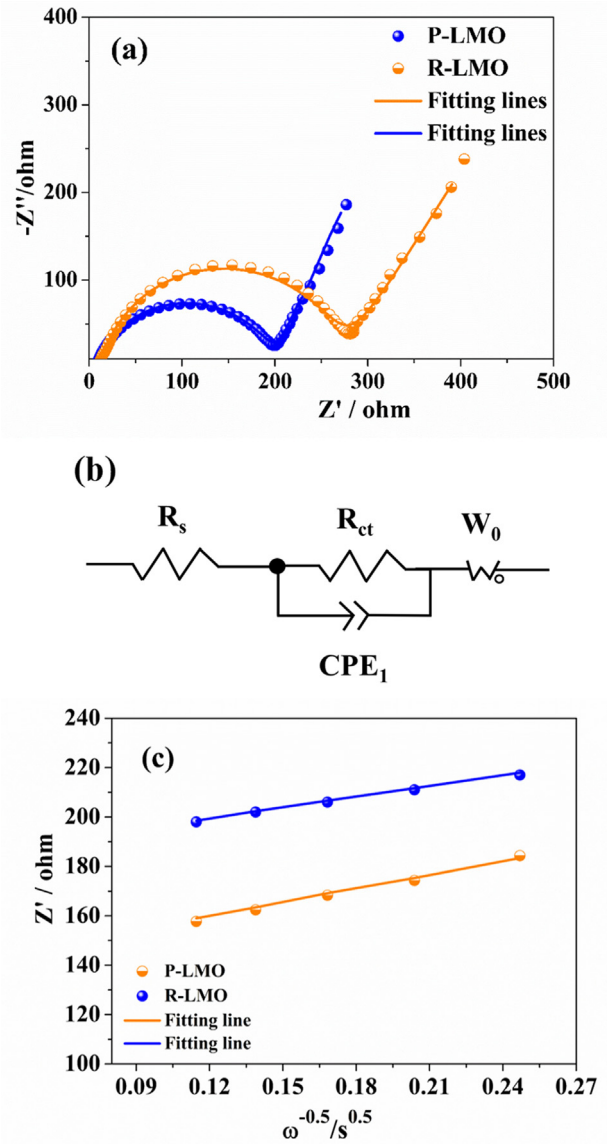

Figure 5. (a) The Nyquist plots of P-LMO and R-LMO samples, (b) The equivalent circuit, (c) Fitting curves of real parts of the complex impedance of the P-LMO and R-LMO samples.

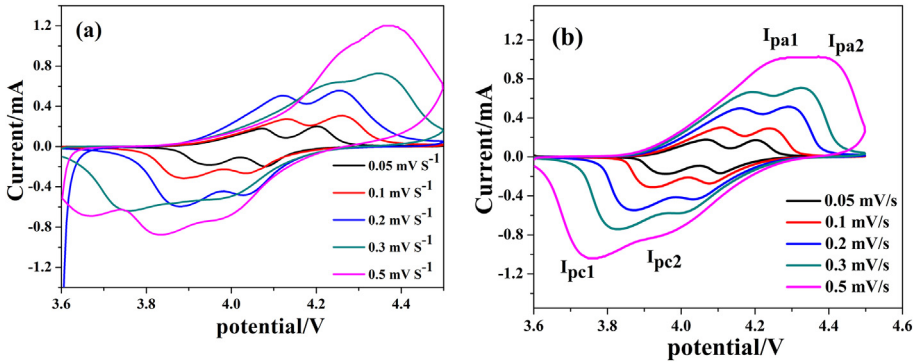

Figure 6. The CV curves of (a) P-LMO and (b)R-LMO samples at virous scan rates from 0.05 mV/s to 0.5 mV/s.

oxidation and reduction peaks due to two stages of intercalation and de-intercalation of Li^+ ions [21, 22]. As seen, the R-LMO sample has a larger peak area than that of P-LMO sample, indicating an improvement of the reversibility due to the fast Li^+ ion transport process due to an increase in the crystallinity of particles.

4. Conclusion

In summary, the spinel $LiMn_2O_4$ cathode material was successfully prepared by recalcination treatment process. In this work, the influence of recalcination treatment on the electrochemical performance of

lithium-ion batteries was studied. The results exhibit that the R-LMO sample has a single crystal truncated-octahedral $LiMn_2O_4$ structure. The high crystallinity performance mainly is due to the selective growth of the (110) and (100) crystal planes promoted by high temperature recalcination treatment. Compared to the P-LMO material, the R-LMO sample possesses better electrochemical reversibility and kinetics from the CV and EIS tests, in which a lower R_{ct} as well as a higher Li ion diffusion coefficient provide more favorable li ion diffusion channels. As a result, the R-LMO sample give the higher cycling and rate performance.

Declarations

Author contribution statement

Jiabin Hao: Conceived and designed the experiments; Performed the experiments; Analyzed and interpreted the data; Contributed reagents, materials, analysis tools or data; Wrote the paper.

Siqi Hao: Conceived and designed the experiments; Analyzed and interpreted the data; Contributed reagents, materials, analysis tools or data.

Mu Xie: Performed the experiments; Analyzed and interpreted the data.

Funding statement

Jiabin Hao was supported by Hebei Province College Students' Science and Technology Innovation Ability Cultivation Program (22E50290D).

Siqi Hao was supported by Natural Science Foundation of Hebei Province (E2022422007).

Data availability statement

Data will be made available on request.

Declaration of interests statement

The authors declare no competing interests.

Additional information

Supplementary content related to this article has been published online at https://doi.org/10.1016/j.heliyon.2022.e12145.

References

[1] M.J. Lee, S. Lee, P. Oh, et al., High performance $LiMn_2O_4$ cathode materials grown with epitaxial layered nanostructure for Li-ion batteries, Nano Lett. 14 (2) (2014) 993–999.

[2] B. Tao, L.C. Yule, E. Daviddi, et al., Correlative electrochemical microscopy of Li-ion (de) intercalation at a series of individual $LiMn_2O_4$ particles, Angew. Chem. 131 (14) (2019) 4654–4659.

[3] C. Zhang, J. Su, T. Wang, et al., Significant improvement on electrochemical performance of $LiMn_2O_4$ at elevated temperature by atomic layer deposition of TiO_2 nanocoating, ACS Sustain. Chem. Eng. 6 (6) (2018) 7890–7901.

[4] A. Van der Ven, C. Marianetti, D. Morgan, et al., Phase transformations and volume changes in spinel $Li_xMn_2O_4$, Solid State Ionics 135 (1-4) (2000) 21–32.

[5] W. Li, G.W. Siqin, Z. Zhu, L. Qi, W.H. Tian, Electrochemical properties of niobium and phosphate doped spherical Li-rich spinel $LiMn_2O_4$ synthesized by ion implantation method, Chin. Chem. Lett. 28 (7) (2017) 1438–1446.

[6] M. Xiang, C.W. Su, L. Feng, et al., Rapid synthesis of high-cycling performance $LiMg_xMn_{2-x}O_4(x\leq0.20)$ cathode materials by a low-temperature solid-state combustion method, Electrochim. Acta 125 (2014) 524–529.

[7] H. Zhao, Y. Nie, Y. Li, et al., Low-cost and eco-friendly synthesis of octahedral $LiMn_2O_4$ cathode material with excellent electrochemical performance, Ceram. Int. 45 (14) (2019) 17183–17191.

[8] L. Yao, Y. Xi, H. Han, et al., $LiMn_2O_4$ prepared from waste lithium-ion batteries through sol-gel process, J. Alloys Compd. 868 (2021), 159222.

[9] H. Zhao, Y. Li, D. Shen, et al., Significantly enhanced electrochemical properties of $LiMn_2O_4$-based composite microspheres embedded with nano-carbon black particles, J. Mater. Res. Technol. 9 (4) (2020) 7027–7033.

[10] H. Zhao, Y. Nie, D. Que, et al., Improved electrochemical properties of $LiMn_2O_4$-based cathode material Co-modified by Mg-doping and octahedral morphology, Materials 12 (17) (2019) 2807.

[11] J. Hao, H. Bai, J. Liu, et al., Synthesis and electrochemical properties of spinel Li (Li0.05Cu0.05Mn1.90) O4 by a flameless combustion method, J. Alloys Compd. 668 (2016) 200–205.

[12] J. Liu, G. Li, H. Bai, et al., Enhanced cycle and rate performances of Li $(Li_{0.05}Al_{0.05}Mn_{1.90})$ O_4 cathode material prepared via a solution combustion method for lithium-ion batteries, Solid State Ionics 307 (2017) 79–89.

[13] C. Jiang, Z. Tang, S. Wang, Z. Zhang, A truncated octahedral spinel $LiMn_2O_4$ as high-performance cathode material for ultrafast and long-life lithium-ion batteries, J. Power Sources 357 (2017) 144–148.

[14] Q. Liu, L. Zhong, Y. Guo, et al., Facile flameless combustion synthesis of high-performance boron-doped $LiMn_2O_4$ cathode with a truncated octahedra, J. Alloys Compd. 874 (2021), 159912.

[15] J.S. Kim, K.S. Kim, W. Cho, et al., A truncated manganese spinel cathode for excellent power and lifetime in lithium-ion batteries, Nano Lett. 12 (12) (2012) 6358–6365.

[16] D.L. Fang, J.C. Li, X. Liu, et al., Synthesis of a Co–Ni doped $LiMn_2O_4$ spinel cathode material for high-power Li-ion batteries by a sol–gel mediated solid-state route, J. Alloys Compd. 640 (2015) 82–89.

[17] S.L. Chou, J.Z. Wang, H.K. Liu, S.X. Dou, Rapid synthesis of $Li_4Ti_5O_{12}$ microspheres as anode materials and its binder effect for lithium-ion battery, J. Phys. Chem. C 115 (2011) 16220–16227.

[18] J. Yao, Y. Li, G. Pan, et al., Electrochemical property of hierarchical flower-like α-Ni $(OH)_2$ as an anode material for lithium-ion batteries, Solid State Ionics 363 (2021), 115595.

[19] L.J. Xi, H.E. Wang, Z.G. Lu, et al., Facile synthesis of porous $LiMn_2O_4$ spheres as positive electrode for high-power lithium-ion batteries, J. Power Sources 198 (2012) 251–257.

[20] Y. Li, J. Yao, E. Uchaker, et al., Sn-doped V_2O_5 film with enhanced lithium-ion storage performance, J. Phys. Chem. C 117 (45) (2013) 23507–23514.

[21] H. Liu, M. Li, M. Xiang, et al., Effects of crystal structure and plane orientation on lithium and nickel co-doped spinel lithium manganese oxide for long cycle life lithium-ion batteries, J. Colloid Interface Sci. 585 (2021) 729–739.

[22] A.M. Hashem, S.M. Abbas, X. Hou, et al., Facile one step synthesis method of spinel $LiMn_2O_4$ cathode material for lithium batteries, Heliyon 5 (7) (2019), e02027.